

# Propulsive matrix of a helical flagellum\*

Zhang He-Peng(张何朋)<sup>a)†</sup>, Liu Bin(刘斌)<sup>b)</sup>, Bruce Rodenborn<sup>c)</sup>, and Harry L. Swinney<sup>c)</sup>

<sup>a)</sup>Department of Physics and Astronomy and Institute of Natural Sciences, Shanghai Jiao Tong University, Shanghai, China

<sup>b)</sup>School of Natural Sciences, University of California, Merced, California, USA

<sup>c)</sup>Department of Physics and Center for Nonlinear Dynamics, University of Texas at Austin, Austin, Texas, USA

(Received 25 July 2014; published online 20 October 2014)

We study the propulsion matrix of bacterial flagella numerically using slender body theory and the regularized Stokeslet method in a biologically relevant parameter regime. All three independent elements of the matrix are measured by computing propulsive force and torque generated by a rotating flagellum, and the drag force on a translating flagellum. Numerical results are compared with the predictions of resistive force theory, which is often used to interpret micro-organism propulsion. Neglecting hydrodynamic interactions between different parts of a flagellum in resistive force theory leads to both qualitative and quantitative discrepancies between the theoretical prediction of resistive force theory and the numerical results. We improve the original theory by empirically incorporating the effects of hydrodynamic interactions and propose new expressions for propulsive matrix elements that are accurate over the parameter regime explored.

**Keywords:** low-Reynolds-number flows, micro-organism dynamics, bacterial swimming

**PACS:** 47.63.-b, 47.63.Gd, 87.17.Jj, 87.16.Qp

**DOI:** 10.1088/1674-1056/23/11/114703

## 1. Introduction

Many types of bacteria<sup>[1–4]</sup> and micro-robots<sup>[5,6]</sup> use rotating helical flagella for propulsive motion. A bacterial flagellum can be modeled as a rigid rotating helix<sup>[2]</sup> with radius  $R$ , pitch  $\lambda$ , length  $L$ , pitch angle  $\theta$ , contour length  $\Lambda = L/\cos\theta$ , and filament radius  $a$ , as shown in Fig. 1. For example, in *Rhizobium lupini*, a flagellum in its normal form is described by the following parameters:  $a = 0.01 \mu\text{m}$ ,  $R = 0.25 \mu\text{m}$ ,  $\lambda = 5.4R$ , and  $L = 4\lambda$ .<sup>[1]</sup> A survey of the current literature<sup>[3,4]</sup> has shown that the pitch of bacterial flagella is typically in the range  $2R < \lambda < 11R$  and the length is in the range  $3\lambda < L < 11\lambda$ .

For a microorganism driven by a helical flagellum rotating about its axis, the Reynolds number  $Re$  is typically  $10^{-4}$  to  $10^{-2}$ , where  $Re = \rho\Omega R^2/\mu$  ( $\Omega$  is the rotation rate;  $\mu$ , the dynamic viscosity;  $\rho$ , the fluid density). At low Reynolds number, a rotating and translating flagellum exerts an axial thrust  $F$  and torque  $\tau$  that are related to the flagellum's axial velocity  $U$  and rotation rate  $\Omega$  by<sup>[7–9]</sup>

$$\begin{pmatrix} F \\ \tau \end{pmatrix} = \begin{pmatrix} A_{11} & A_{12} \\ A_{12} & A_{22} \end{pmatrix} \cdot \begin{pmatrix} U \\ \Omega \end{pmatrix}. \quad (1)$$

The symmetric  $2 \times 2$  propulsive matrix in Eq. (1) depends only on the geometry of the flagellum. The elements of the propulsive matrix can be determined by measuring the axial thrust  $F$  and torque  $T$  for a rotating non-translating flagellum, and the axial drag  $D$  on a translating non-rotating flagellum.

The propulsive matrix can be calculated by the resistive force theory developed by Gray and Hancock<sup>[10]</sup> and Lighthill.<sup>[11]</sup> Their theory decomposes a flagellum into short segments and calculates the fluid force on each element, ignoring the hydrodynamic interactions between different parts of a flagellum. Integrating over the contour length of the flagellum leads to algebraic expressions that relate force and torque to the axial velocity and rotation rate of a helical flagellum. Recent experimental and numerical studies have shown that these expressions are only qualitatively correct.<sup>[4,12–14]</sup> In the parameter regime relevant to bacteria, predictions of resistive force theory differ from experiments by at least a factor of two.<sup>[13]</sup> Further, numerical simulations, experiments, and an asymptotic analysis show that the thrust and drag for long helices vary as  $(L/R)/\ln(L/R)$  rather than as  $L/R$  as predicted by resistive force theory. The failures of resistive force theory have been attributed to its neglect of hydrodynamic interactions.

Despite its quantitative limitations, resistive force theory has been successfully used as a simple and convenient framework to interpret biological self-propulsion, including sperm,<sup>[15]</sup> *Caenorhabditis elegans*,<sup>[16]</sup> *Chlamydomonas reinhardtii*,<sup>[17]</sup> swimmers in a granular material,<sup>[18,19]</sup> and snake motion.<sup>[20]</sup> In these studies, rather than using the drag coefficients given in the original theory,<sup>[10,11]</sup> the researchers have treated the coefficients as free parameters that were adjusted to fit the observations, such as sperm trajectories in

\*Project supported by the National Natural Science Foundation of China (Grant No. 11104179), the Shanghai Pujiang Program, China (Grant No. 12PJ1405400), the Program for Professor of Special Appointment (Eastern Scholar) at Shanghai Institutions of Higher Learning, China (Grant No. SHDP201301), and the Innovation Program of Shanghai Municipal Education Commission, China (Grant No. 14ZZ030).

†Corresponding author. E-mail: [hepeng\\_zhang@sjtu.edu.cn](mailto:hepeng_zhang@sjtu.edu.cn)

Ref. [15] and swimming speed of *C. elegans* in Ref. [16].

Here we explore the possibility of adapting resistive force theory for accurate prediction of the propulsive matrix of a helical flagellum. To this end, we use slender body theory and the regularized Stokeslet method to compute the propulsive matrix of bacterial flagella in a biologically relevant regime. Guided by the numerical results, we empirically incorporate effects of hydrodynamic interactions into resistive force theory and obtain parametrized expressions that quantitatively describe the propulsive matrix for a wide range of bacterially relevant flagella.

## 2. Methods

In this section, we briefly review the formulation of numerical methods and resistive force theory. Details of the numerical implementation can be found in Ref. [4].

### 2.1. Stokeslet and regularized Stokeslet methods

A flow at a low Reynolds number is governed by the Stokes equations.<sup>[8,9]</sup> The linearity of the Stokes equations allows for important theoretical simplifications because the flow dynamics can be solved using a Green's function method. The solution for the fluid velocity, or Stokeslet,<sup>[10]</sup> resulting from a point-force at the origin,  $f\delta(\mathbf{r})$ , is given by<sup>[7-9]</sup>

$$\mathbf{u}(\mathbf{r}) = \mathbf{f} \cdot \mathbb{J}(\mathbf{r}), \quad (2)$$

where  $\mathbb{J}(\mathbf{r})$  is the Oseen tensor, defined as

$$\mathbb{J}(\mathbf{r}) \equiv \frac{1}{8\pi\mu} \left( \frac{\mathbb{I}}{|\mathbf{r}|} + \frac{\mathbf{r}\mathbf{r}^T}{|\mathbf{r}|^3} \right), \quad (3)$$

and  $\mu$  is the dynamic viscosity of the fluid. Lorentz showed that the response to a continuous force distribution from an immersed body can be found by superposing these Stokeslets;<sup>[21]</sup> that is,

$$\mathbf{u}(\mathbf{r}) = \int \mathbf{f}(\mathbf{r}') \cdot \mathbb{J}(\mathbf{r} - \mathbf{r}') d\mathbf{r}'. \quad (4)$$

The hydrodynamic theory discussed above includes Dirac delta functions, which are difficult to calculate computationally. The regularized Stokeslets method<sup>[4,22]</sup> eases the evaluation of integrals with singular kernels by replacing the delta distribution of forces,  $\delta(\mathbf{r})$ , with a smooth, localized distribution

$$\phi_\varepsilon(\mathbf{r}) = \frac{15\varepsilon^4}{8\pi(r^2 + \varepsilon^2)^{7/2}}, \quad (5)$$

where  $r = |\mathbf{r}|$  and regularization parameter  $\varepsilon$  is assumed to be small. This parameter  $\varepsilon$  prevents non-integrable kernels, but also has a physical meaning of representing surface area over which the force is distributed. In the regularized Stokeslets method, for  $N$  regularized point forces  $\mathbf{f}\phi_\varepsilon(\mathbf{r}_n)$  at locations

$\mathbf{r}_n$  on the surface of a body in motion, the fluid velocity at any point  $\mathbf{r}$  is

$$u_j(\mathbf{r}) = \frac{1}{8\pi\mu} \sum_{n=1}^N \sum_{i=1}^3 S_{ij}^\varepsilon(\mathbf{r} - \mathbf{r}_n) f_{n,i} A_n, \quad (6)$$

where  $A_n$  are quadrature weights, and the regularized Green's function  $S_{ij}^\varepsilon$  is

$$S_{ij}^\varepsilon(\mathbf{r}) = \frac{\delta_{ij}(r^2 + 2\varepsilon^2) + r_i r_j}{(r^2 + \varepsilon^2)^{3/2}}. \quad (7)$$

We can determine the strength of the  $N$  regularized Stokeslets,  $f_{n,i}$ , from the velocity at the surface of the body,  $u_j(\mathbf{r})$ , by inverting Eq. (6). From  $f_{n,i}$ , the force and torque on the body can be computed. Details of the numerical implementation of the regularized Stokeslets method can be found in Refs. [4] and [22].

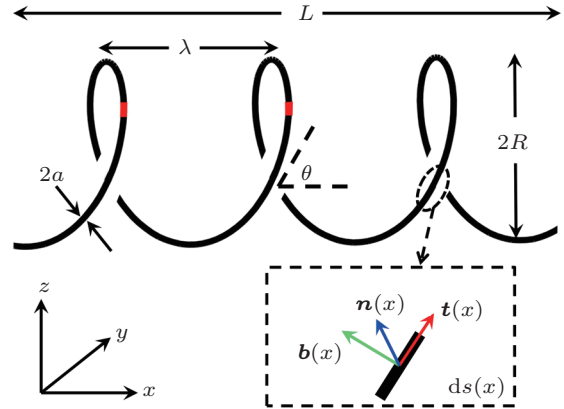


**Fig. 1.** Schematic program of a flagellum with filament radius  $a$ , helix radius  $R$ , pitch  $\lambda$ , axial length  $L$ , filament contour length  $\Lambda = \lambda / \cos \theta$ , and pitch angle  $\theta$ , where  $\tan \theta = 2\pi R / \lambda$ . A filament segment  $ds$  is shown in the inset with tangential, normal, and bio-normal directions denoted as  $\hat{t}(x)$ ,  $\hat{n}(x)$ ,  $\hat{b}(x)$ , respectively. The two filament segments in red illustrate nearby points affected by hydrodynamic interactions (see text).

### 2.2. Slender body theory

Bacteria flagella are slender, and their filament radius  $a$  is usually much smaller than other geometric parameters. Taking advantage of this slenderness, Lighthill developed slender body theory,<sup>[11]</sup> which represents a flagellum with an arrangement of Stokeslets and doublets along the flagellum's centerline. Since dipolar fields fall off as  $r^{-2}$  while Stokeslets fall off as  $r^{-1}$ , Lighthill reasoned there should be some intermediate distance  $q$  from any given point on the flagellum where only the dipoles within  $q$  are important in determining the flow at that point, although all of the Stokeslets on the centerline must be considered because they are longer ranged. He showed that the sum of the near and far field solutions for the induced fluid flow on a given segment could be made independent of  $q$  by the choice of dipoles of the form<sup>[9,11]</sup>

$$-\frac{a^2 \mathbf{f}_\perp(s)}{4\mu}, \quad (8)$$

where  $\mathbf{f}_\perp(s)$  is the component of the Stokeslet strength  $\mathbf{f}$  in the plane perpendicular to the flagellum's centerline at a location  $s$  along the centerline of the flagellum.<sup>[11,23]</sup> This combination of a Stokeslet plus a dipole determines the flow induced by each element of the flagellum. Lighthill showed the local velocity of a segment of the helix located at  $s$  is related to the force per unit length (i.e., Stokeslet strength) along the filament  $\mathbf{f}(s)$  by

$$\mathbf{u}(s) = \frac{\mathbf{f}_\perp(s)}{4\pi\mu} + \int_{|\mathbf{r}_0(s',s)|>\delta} \mathbf{f}(s') \cdot \mathbb{J}(\mathbf{r}_0) ds', \quad (9)$$

where  $\delta = a\sqrt{\epsilon}/2$  is the "natural cutoff"<sup>[9,11]</sup> and  $\mathbb{J}$  is given by Eq. (3). We evaluate Eq. (9) using the rectangular rule of numerical integration to calculate the thrust, torque, and drag for flagella; the numerical details can be found in Ref. [4].

Consider a flagellum parametrized by  $s$  as in Eq. (9) with a length  $L$ . For a sufficiently long flagellum ( $L \gg R$  and  $L \gg \lambda$ ), the end effects are minimal and we have translational invariance. Therefore, the force per unit length in Eq. (9),  $\mathbf{f}(s)$ , does not depend on  $s$ . In this case, we have shown in Ref. [4] that the following scaling relationships for thrust, torque and drag hold in the limit that  $L \rightarrow \infty$ :

$$F \propto \frac{L}{\ln(L/R)}, \quad (10)$$

$$T \propto L, \quad (11)$$

$$D \propto \frac{L}{\ln(L/R)}. \quad (12)$$

### 2.3. Resistive force theory for a helical flagellum

Obtaining numerical predictions from slender body theories requires inversions of an integral equation, such as Eq. (9). Such computations were difficult when the original theories were developed, so a further simplification was sought by considering each segment of the flagellum as an independent slender rod, a model now known as the resistive force theory.<sup>[10,11]</sup> The resistance of the fluid to the slender rod's motion is calculable if the local coefficient of drag for the segment and its velocity are known. The drag is expressed in terms of normal and tangential drag coefficients per unit length,  $C_n$ , and  $C_t$ , respectively. The total force and torque for any motion of the flagellum is then obtained by an integration of the force and torque from each small segment. Resistive force theory then predicts the thrust, torque, and drag on a flagellum as given by

$$F = (\Omega R) (C_n - C_t) \sin \theta \cos \theta \frac{L}{\cos \theta}, \quad (13)$$

$$T = (\Omega R^2) (C_n \cos^2 \theta + C_t \sin^2 \theta) \frac{L}{\cos \theta}, \quad (14)$$

$$D = U (C_n \sin^2 \theta + C_t \cos^2 \theta) \frac{L}{\cos \theta}, \quad (15)$$

where  $F$  and  $T$  are the axial force and torque for a rotating, non-translating flagellum, and  $D$  is the axial drag on a non-rotating flagellum. These three quantities uniquely determine

the elements of the propulsive matrix (1) as

$$A_{11} = D/U, \quad (16)$$

$$A_{12} = F/\Omega, \quad (17)$$

$$A_{22} = T/\Omega. \quad (18)$$

Equations (13)–(15) predict that thrust, torque, and drag depend linearly on the axial length  $L$ , which is in contradiction with predictions of slender body theory, Eqs. (10)–(12).

Evaluating Eqs. (13)–(15) requires determining the local drag coefficients. Two sets of drag coefficients are commonly used in the literature, those by Gray and Hancock<sup>[10]</sup> and those by Lighthill.<sup>[11]</sup> We focus on the latter.

Lighthill's analysis is based on his slender body theory formulation for the zero-thrust swimming speed of a helical flagellum. He obtained

$$C_t = \frac{2\pi\mu}{\ln \frac{0.18\lambda}{a \cos \theta}}, \quad (19)$$

$$C_n = \frac{4\pi\mu}{\ln \frac{0.18\lambda}{a \cos \theta} + 1/2}. \quad (20)$$

Equations (13)–(15) along with drag coefficients expressions, Eqs. (19) and (20), predict the elements of a flagellum's propulsive matrix, which we test using numerical simulations in the next section.

## 3. Results

In this section, we present the main results of our study. First, we compare the theory to the numerical results and show that the current resistive force theory is inadequate to describe the propulsive matrix. Guided by this comparison, we propose new empirical expressions for the propulsive matrix and relate the parameters in the new expressions to the geometric measures of the helical flagellum. Finally, we show that our empirical expressions accurately predict the hydrodynamic efficiency of biologically relevant flagella.

### 3.1. New expressions for thrust, torque, and drag

Our results computed for the thrust, torque, and drag for flagella with filament radii  $a = R/10$  and  $a = R/30$  are shown in Fig. 2 as a function of helical pitch ( $R < \lambda < 19R$ ); the axial length is  $L = 30R$ . The numerical results from slender body theory and the regularized Stokeslet method<sup>[22]</sup> are in excellent agreement. In Ref. [4], we showed that predictions of slender body theory and the regularized Stokeslet method compare well with experimental measurements. Since the computational cost of slender body theory is much less than that of the regularized Stokeslet method, we will use slender body theory for numerical calculations for the rest of the paper.

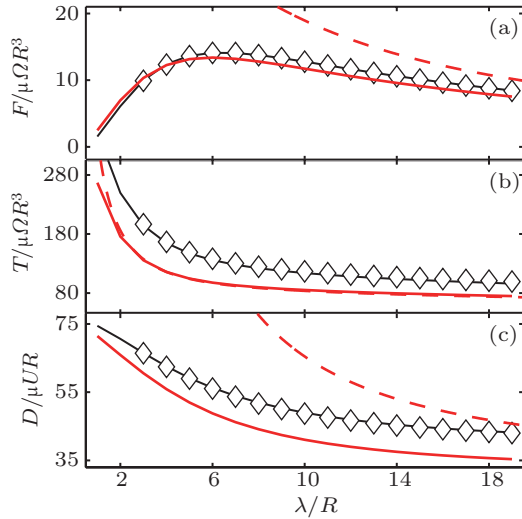


**Fig. 2.** Nondimensional thrust (a), torque (b), and drag (c) for flagella with filament radii  $a = R/10$  (black) and  $a = R/30$  (red), as a function of pitch  $\lambda$  (normalized by the helix radius  $R$ ): regularized Stokeslet method (diamonds), slender body theory of Lighthill (solid black/red lines), and resistive force theory of Lighthill (dashed red lines). (Here,  $L = 30R$ ).

The resistive force theory prediction compares poorly with the numerical results. For long wavelengths,  $\lambda > 10R$ , theoretical predictions of thrust agree qualitatively with the other data within a factor of 2. However, for flagella with  $\lambda < 10R$ , theoretical predictions for thrust diverge significantly from experiments and simulations. Resistive force theory (13) predicts that  $F$  increases as the helical pitch decreases, while other methods show that  $F$  has a maximum at approximately  $\lambda = 5.5R$ . The theory also predicts that the drag  $D$  is larger by about a factor of two. Theoretical predictions for torque (red dashed line in Fig. 2(b)) are close to simulation results (solid line), but such an agreement is coincidental for this particular set of parameters. The results in Fig. 2 also show interesting filament radius dependence. An increase in the filament radius from  $a = R/30$  (red lines) to  $a = R/10$  (black lines) barely changes the thrust (less than 5%) but results in significant increases in both torque ( $\sim 30\%$ ) and drag ( $\sim 20\%$ ).<sup>[4]</sup>

Despite its lack of quantitative accuracy, as shown in Fig. 2, resistive force theory provides a simple and convenient framework to interpret biological self-propulsion. In order to reproduce experimental observations, researchers have treated drag coefficients in Eqs. (13)–(15) as free fitting parameters. For example, Sznitman *et al.*<sup>[16]</sup> showed that *C. elegans* swimming motility can be described by resistive force theory with a ratio of drag coefficients  $C_n/C_t = 1.4$ , and Friedrich *et al.*<sup>[15]</sup> found  $C_n/C_t$  to be 1.8 in studies of sperm. In our study, it is difficult to find a pair of drag coefficients that can accurately predict all three quantities: thrust, torque, and drag. A third parameter,  $S_{\text{drag}}$ , has to be introduced to the expression for drag, Eq. (15); the origin of  $S_{\text{drag}}$  will be discussed in the next sub-section. By combining this point with asymptotic scal-

ings (Eqs. (10), (11), and (12)), we propose new expressions for thrust, torque, and drag as

$$F = (\Omega R) [(C_n - C_t) \sin \theta \cos \theta] \left[ \frac{L}{\cos \theta} \right] \left[ \frac{\ln 30}{\ln(L/R)} \right], \quad (21)$$

$$T = (\Omega R^2) [C_n \cos^2 \theta + C_t \sin^2 \theta] \left[ \frac{L}{\cos \theta} \right], \quad (22)$$

$$D = S_{\text{drag}} V [C_n \sin^2 \theta + C_t \cos^2 \theta] \left[ \frac{L}{\cos \theta} \right] \left[ \frac{\ln 30}{\ln(L/R)} \right]. \quad (23)$$

In Eq. (21) and (23), a factor of  $\ln 30$  is included because our study covers the biologically relevant regime:  $20R < L < 50R$ . In this regime, the ratio of  $\ln 30 / \ln(L/R)$  is around one (0.86 to 1.14).

### 3.2. Parametrization of $C_n$ , $C_t$ , and $S_{\text{drag}}$

For a given flagellum, we can obtain  $C_n$ ,  $C_t$  and  $S_{\text{drag}}$  using the computed results for thrust, torque, and drag along with Eqs. (21) and (23). The results from a set of flagella with various wavelengths are shown by symbols in Fig. 3. Lighthill's expressions for drag coefficients, dashed lines in Fig. 3(a), diverge from the computational results significantly for flagella with small pitch, which is consistent with the results in Fig. 2(a). The extracted  $S_{\text{drag}}$  (symbols in Fig. 3(b)), has a value around 0.5 and increases nonlinearly with helical pitch.

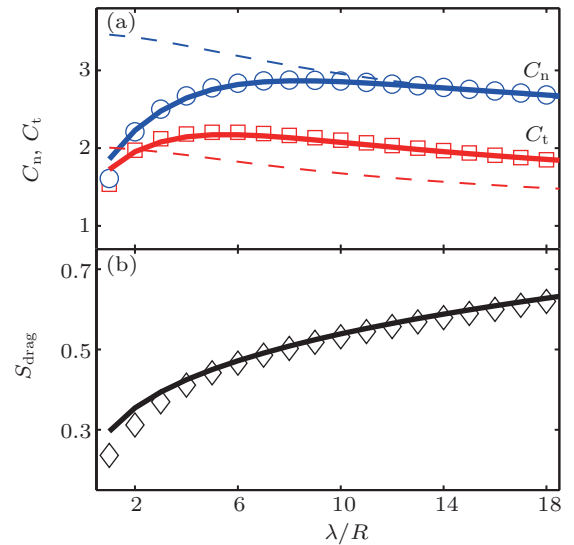


**Fig. 3.** (a) Drag coefficients  $C_n$  (circles) and  $C_t$  (squares) from simulations with  $a = (1/20)R$ ,  $L = 30R$ , and  $R < \lambda < 20R$ . The solid lines are the new parametrization of these coefficients provided in Eqs. (24) and (25). Lighthill's expression (Eqs. (19) and (20)) for  $C_n$  and  $C_t$  are shown as dashed lines. (b) The drag scaling factor extracted from the same simulations (diamonds) with the parametrization from Eq. (26) plotted as the solid line.

The origin of  $S_{\text{drag}}$  can be understood qualitatively as follows. A point force  $\mathbf{f}$  generates a flow field at a location  $\mathbf{r}$  away from itself as

$$\mathbf{u}(\mathbf{r}) = \frac{1}{8\pi\mu} \left( \frac{\mathbb{I}}{r} + \frac{\mathbf{r}\mathbf{r}}{r^3} \right) \cdot \mathbf{f}.$$

If  $\mathbf{r}$  is in the direction of  $\mathbf{f}$ , then the generated flow is  $\mathbf{u}_{\parallel} = \mathbf{f}/4\pi\mu r$ . If  $\mathbf{r}$  is perpendicular to  $\mathbf{f}$ , then the generated flow is  $\mathbf{u}_{\perp} = \mathbf{u}_{\parallel}/2$ . This means that the flow induced by a Stokeslet is spatially anisotropic: the flow at a location in the Stokeslet direction is twice as strong as the flow at an equally-distant location in the perpendicular direction. When a flagellum translates in the  $\hat{x}$  direction, as in our results computed for the drag, local velocities of these segments are also in  $\hat{x}$  direction, meaning that the representative Stokeslets have a large component in the  $\hat{x}$  direction. When the flagellum rotates in the axial direction, as in our force and torque computations, local velocities are perpendicular to the  $\hat{x}$  direction, so the associated Stokeslets have a larger component perpendicular to the  $\hat{x}$  direction than parallel to the axis. Consequently, hydrodynamic interaction between flow induced by segments of a flagellum is stronger if the flagellum translates as opposed to when it rotates. This is analogous to the case of translating a slender cylinder along and perpendicular to its axis, where the ratio of the two drag coefficients is approximately 2 for long slender cylinders.<sup>[9]</sup>

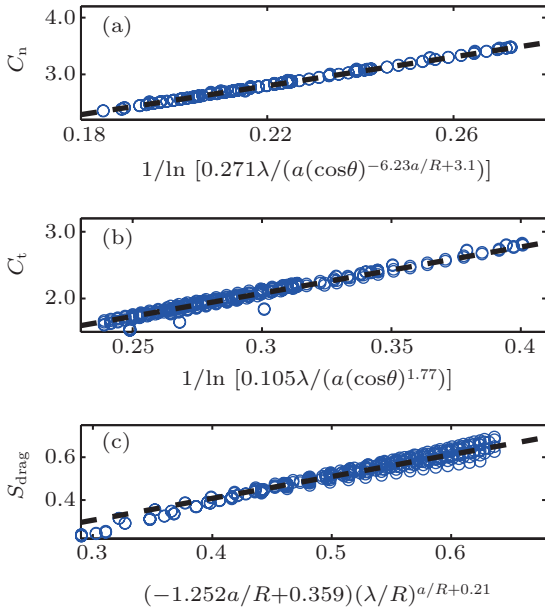


**Fig. 4.** Collapse of  $C_n$  (a),  $C_t$  (b), and  $S_{\text{drag}}$  (c) (symbols) according to Eqs. (25) to (26) (dashed lines). Our study covers a biologically relevant parameter regime of  $(1/30)R < a < (1/10)R$ ,  $R < \lambda < 20R$ , and  $20R < L < 50R$ .

Next, we parametrize  $C_n$ ,  $C_t$  and  $S_{\text{drag}}$  as functions of a flagellum's geometric parameters. To that end, we compute thrust, torque, and drag for flagella in a biologically relevant regime where  $(1/30)R < a < (1/10)R$ ,  $R < \lambda < 20R$ , and  $20R < L < 50R$ . From each geometry,  $C_n$ ,  $C_t$ , and  $S_{\text{drag}}$  are computed from Eqs. (21) to (23). We find that  $C_n$ ,  $C_t$ , and  $S_{\text{drag}}$  mainly depend on three geometric parameters  $\lambda$ ,  $a$ , and  $R$ . The dependence is simple enough to be parametrized. In Fig. 4, results for  $C_n$ ,  $C_t$ , and  $S_{\text{drag}}$  are plotted as functions of

scaled variables, and we find that the following expressions describe the data well:

$$C_t = 2.21\pi\mu/\ln\left[\frac{0.105\lambda}{a(\cos\theta)^{1.77}}\right], \quad (24)$$

$$C_n = 4.05\pi\mu/\ln\left[\frac{0.271\lambda}{a(\cos\theta)^{-6.23a/R+3.1}}\right], \quad (25)$$

$$S_{\text{drag}} = (-1.252a/R + 0.359)(\lambda/R)^{a/R+0.21}, \quad (26)$$

which are the lines in the figure.

### 3.3. Hydrodynamic efficiency

Equations (21) to (23) coupled with Eqs. (24) to (26) form a closed system that can predict thrust, torque, and drag for any flagellum. We test the accuracy of our scheme by computing the hydrodynamic efficiency as defined by Purcell<sup>[3,24]</sup>

$$\varepsilon = \frac{A_{12}^2}{4A_{11}A_{22}} = \frac{F^2U}{4TD\Omega}, \quad (27)$$

where  $A_{11}$ ,  $A_{12}$ ,  $A_{22}$  are elements of the propulsion matrix. We compute this efficiency for nine forms of bacterial flagella observed in nature, which varies in radius and pitch angle. The geometric parameters of the flagella, hydrodynamic efficiency from numerical simulations  $\varepsilon_n$ , and efficiency given by our parametrization  $\varepsilon_p$  are shown in Table 1. In all our calculations, we use a filament radius  $a = 0.01 \mu\text{m}$  and a contour length  $\Lambda = 10 \mu\text{m}$ . The difference between  $\varepsilon_p$  and  $\varepsilon_n$  is less than 10% except for “coiled” flagella which have very small  $\lambda/R$ . In the regime of small  $\lambda/R$ , hydrodynamic interactions are strong and our parametrization is not accurate. For both Peritrichous and Monotrichous flagella, the “normal” form has the highest efficiency, which is consistent with a recent study by Spagnolie and Lauga.<sup>[3]</sup>

To further test the parametrization scheme, we compute the hydrodynamic efficiency of two flagella from Table 1 that have the same filament radius  $a = 0.01 \mu\text{m}$  and contour length  $\Lambda = 10 \mu\text{m}$ , but different helical radii—Peritrichous normal form ( $R = 0.221 \mu\text{m}$ ) and curly form ( $R = 0.123 \mu\text{m}$ ). The helical pitch is allowed to vary from 0 to 90 degrees, and in both cases, an optimal efficiency appears around  $\theta \approx 41^\circ$ , as shown in Fig. 5. We also see that a larger helix radius  $R$  in the normal form leads to a higher efficiency. This can be qualitatively understood as a consequence of change in axial length  $L$ . From Eqs. (21)–(23) and the definition of hydrodynamic efficiency Eq. (27), we find hydrodynamic efficiency depends on the axial length as

$$\varepsilon \propto \frac{1}{\ln(L/R)}.$$

Since we fixed the contour length ( $\Lambda^2 = (2\pi R)^2 + L^2$ ), a smaller helix radius  $R$  leads to a larger axial length  $L$  and, therefore a lower hydrodynamic efficiency.

**Table 1.** Geometric parameters and hydrodynamic efficiency of naturally observed bacterial flagella. Geometric parameters were extracted from Spagnolie and Lauga.<sup>[3]</sup> In all our computations, we use a filament radius  $r = 0.01 \mu\text{m}$  and a contour length  $\Lambda = 10 \mu\text{m}$ .

	Peritrichous					Monotrichous			
	Normal	Semi-coiled	Curly	Curly-II	Coiled	Normal	Semi-coiled	Curly	Coiled
$R/\mu\text{m}$	0.221	0.257	0.128	0.074	0.689	0.170	0.298	0.132	0.405
$\lambda/\mu\text{m}$	2.284	1.167	1.029	0.961	0.784	1.402	1.177	0.971	1.059
$\epsilon_n/10^{-3}$	8.749	7.232	7.239	4.661	0.748	8.347	6.504	7.257	3.715
$\epsilon_p/10^{-3}$	8.901	7.818	7.041	4.343	1.522	8.349	7.251	7.121	4.56

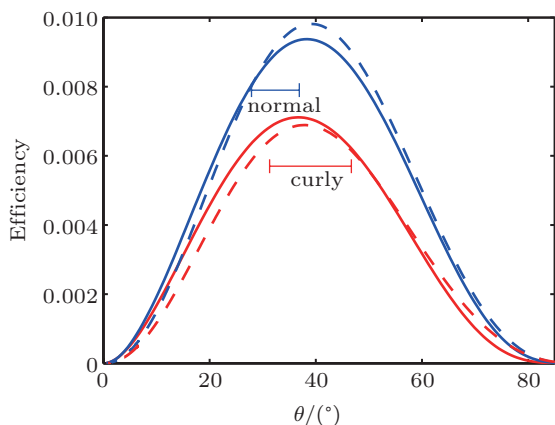


**Fig. 5.** Hydrodynamic efficiency of two sets of flagella ( $R = 0.221 \mu\text{m}$ , upper curves, and  $R = 0.123 \mu\text{m}$ , lower curves). In both cases, the filament radius is  $a = 0.01 \mu\text{m}$  and the contour length is  $\Lambda = 10 \mu\text{m}$ . The solid lines are our numerical simulation results and the dashed lines are computed from our new resistive force parametrization scheme. The range of pitch angles for the Peritrichous normal and curly forms are indicated below the blue and red curves, respectively.

#### 4. Conclusions

Current and previous<sup>[4]</sup> studies have shown that resistive force theory in its original form is not sufficient to describe swimming with a helical flagellum. Neglecting hydrodynamic interactions between different parts of a flagellum in resistive force theory leads to three types of discrepancies. First, the theory significantly overestimates thrust for flagella with small pitch ( $\lambda < 8R$ ), as shown in Fig. 2. Second, resistive force theory overestimates the drag force for all flagella by a factor of about two. Third, resistive force theory predicts that thrust, torque, and drag all scale linearly with axial length  $L$ , but a theoretical analysis including hydrodynamic interactions shows that only torque scales linearly, while thrust  $F$  and drag  $D$  scale as  $L/\ln(L/R)$ .

We have improved the original theory by empirically incorporating the effects of hydrodynamic interactions, and we have proposed new expressions for propulsive matrix el-

ements, Eqs. (21)–(23). The drag coefficients ( $C_n$  and  $C_t$ ) and the new parameter ( $S_{\text{drag}}$ ) in our expressions have been parametrized as functions of geometric parameters, Eq. (24)–(26). We have shown that our parametrization scheme is quantitatively accurate for a wide range of bacterial flagella.

#### References

- [1] Scharf B 2002 *J. Bacteriology* **184** 5979
- [2] Darnton N C, Turner L, Rojevsky S and Berg H C 2007 *J. Bacteriology* **189** 1756
- [3] Spagnolie S E and Lauga E 2011 *Phys. Rev. Lett.* **106** 058103
- [4] Rodenborn B, Chen C H, Swinney H L, Liu B and Zhang H P 2013 *Proc. Natl. Acad. Sci. USA* **110** E338
- [5] Zhang L, Abbott J J, Dong L X, Peyer K E, Kratochvil B E, Zhang H X, Bergeles C and Nelson B J 2009 *Nano Lett.* **9** 3663
- [6] Nelson B J, Kaliakatsos I K and Abbott J J 2010 *Annu. Rev. Biomed. Eng.* **12** 55
- [7] Happel J and Brenner H 1965 *Low Reynolds Number Hydrodynamics* (Englewood Cliffs, NJ: Prentice Hall)
- [8] Kim S and Karrila J S 1991 *Microhydrodynamics: Principles and Selected Applications* (Boston: Butterworth-Heinemann)
- [9] Lauga E and Powers T R 2009 *Rep. Prog. Phys.* **72** 096601
- [10] Gray J and Hancock G T 1955 *J. Exp. Biol.* **32** 802
- [11] Lighthill J 1976 *SIAM Rev.* **18** 161
- [12] Chattopadhyay S, Moldovan R, Yeung C and Wu X L 2006 *Proc. Natl. Acad. Sci. USA* **103** 13712
- [13] Chattopadhyay S and Wu X L 2009 *Biophys. J.* **96** 2023
- [14] Liu B, Breuer K S and Powers T R 2013 *Phys. Fluids* **25** 061902
- [15] Friedrich B M, Riedel-Kruse I H, Howard J and Julicher F 2010 *Journal of Experimental Biology* **213** 1226
- [16] Sznitman J, Shen X, Sznitman R and Arratia P E 2010 *Phys. Fluids* **22** 121901
- [17] Bayly P V, Lewis B L, Ranz E C, Okamoto R J, Pless R B and Dutcher S K 2011 *Bio-phys. J.* **100** 2716
- [18] Maladen R D, Ding Y, Umbanhowar P B, Kamor A, and Goldman D I 2011 *Journal of the Royal Society Interface* **8** 1332
- [19] Ding Y, Sharp S S, Wiesenfeld K and Goldman D I 2013 *Proc. Natl. Acad. Sci. USA* **110** 10123
- [20] Hu D L, Nirody J, Scott T and Shelley M J 2009 *Proc. Natl. Acad. Sci. USA* **106** 10081
- [21] Lorentz H A 1996 *J. Eng. Math.* **30** 19
- [22] Cortez R, Fauci L and Medovikov A 2005 *Phys. Fluids* **17** 031504
- [23] Lighthill J 1996 *J. Eng. Math.* **30** 25
- [24] Purcell E M 1997 *Proc. Natl. Acad. Sci. USA* **94** 11307